Seasonal thermal signatures of heat transfer by water exchange in an underground vault

Frédéric Perrier, Pierre Morat, Toshio Yoshino, Osam Sano, Hisashi Utada, Olivier Gensane, Jean-Louis Le Mouël

Geophys. J. Int. (2004) **158,** 372–384 doi: 10.1111/j.1365-246X.2004.02292.x

Seasonal thermal signatures of heat transfer by water exchange in an underground vault

Frédéric Perrier,[1] Pierre Morat,[2] Toshio Yoshino,[3] Osam Sano,[3] Hisashi Utada,[3] Olivier Gensane[3] and Jean-Louis Le Mouël[2]

[1]*Service Radioanalyses, Chimie, Environnement, Département Analyse, Surveillance, Environnement, Commissariat à l'énergie Atomique, B.P. 12,* 91680 *Bruyères-le-Châtel, France. E-mail: frederic.perrier@cea.fr*
[2]*Laboratoire de Géomagnétisme, Institut de Physique du Globe, 4, Place Jussieu,* 75005 *Paris, France*
[3]*Earthquake Research Institute, University of Tokyo, Yoyoi 1-1-1, Bunkyo-ku, Tokyo* 113, *Japan*

Accepted 2004 March 17. Received 2004 March 2; in original form 2002 July 5

SUMMARY

The temperature of a 10-point vertical profile at the rock–atmosphere interface has been monitored since 2000 September in an underground vault at Aburatsubo, Japan, where resistivity variations have been reported in association with earthquakes. The non-ventilated vault is characterized by an annual temperature variation of about 1.2 °C peak to peak, compatible with thermal diffusion in the surrounding tuff rock, and by a long-term temperature increase of about 0.1 °C per year, possibly due to a local or global climate change. Owing to a careful relative calibration of the 10 thermistors used in this experiment, these data establish that the ceiling temperature is higher than the floor temperature by 0.04 to 0.28 °C. Transient temperature variations are observed in association with human presence or with typhoons, with a characteristic spatial pattern revealing structural heterogeneity. Variations with periods ranging from 1 day to 1 week, with an amplitude two time larger and a phase advance on the floor with respect to the ceiling, are observed from November to May. Variations with periods larger than 1 week, with an amplitude two times smaller and a phase lag on the floor with respect to the ceiling, are observed from June to October. These cycles are linked to the sign of the seasonal heat flux. We propose an interpretation in which heat transfer in the cavity is dominated by diffusion of water vapour from June to October (heat flux downwards, summer regime) and by convective water transport from November to May (heat flux upwards, winter regime). The water flow inferred from this model can be used to predict the water saturation of the rock as a function of time. Because of a permanent radiative heat flux from top to bottom, the upward water flow in the winter regime is larger than the downward water flow in the summer regime, resulting in a slow depletion of water from the rock below the cavity. This unbalanced water flow could contribute to an observed steady secular increase of rock resistivity, and possibly also to the long-term temperature increase of 0.1 °C per year. It is important to understand these processes in the context of underground geophysical observatories, underground waste storage and contaminant transport, as well as for the preservation of cultural items such as cave paintings.

Key words: atmospheric effects, heat generation and transport, non-linear dynamics, thermal properties, water/energy interactions.

INTRODUCTION

Understanding the thermodynamics of underground cavities is a pre-requisite in many applications of economic or cultural importance. Assessing the stability of underground nuclear waste storage sites is currently a major issue and the effect of artificial heat sources has been studied in dedicated experiments (e.g. Birkholzer & Tsang 2000; Witherspoon 2000). While the main results of these experiments, and in particular the artificial heat-driven water flows, can be accounted for in the framework of thermohydromechanical models (e.g. Tsang 2000), the long-term impact and the effects of structural heterogeneity remain poorly known. Similarly, the preservation of precious cultural heritage items such as cave paintings (e.g. Hoyos *et al.* 1998; Sanchez-Moral *et al.* 1999) or rare underground

ecosystems (De Freitas & Littlejohn 1987) relies on the knowledge of heat and moisture exchange between the partially saturated rocks and the atmosphere.

A possible method for assessing the water content of rocks is the measurement of electrical resistivity. Surprising observations have been collected at the underground crustal deformation observatory in Aburatsubo, Japan, where the apparent resistivity of the rock has been monitored since 1968 (Yamazaki 1975; Utada *et al.* 1998; Yoshino *et al.* 1998). Annual relative variations of resistivity $\Delta\rho/\rho$ of the order of 1 per cent are observed, on top of a linear increase of about 0.5 per cent per year. A striking feature of the data is the presence of co-seismic changes, with a sign that exhibits seasonal variations: these are positive from November to April and negative from May to October.

Preliminary temperature measurements at various depths in the Aburatsubo cavity led workers to suspect a crucial role for the heat flux in the observed resistivity variations (Utada *et al.* 1998). Because of the large latent heat of vaporization of water, temperature measurements are a powerful tool for exploring water exchanges between rocks and the atmosphere (Morat *et al.* 1999; Brüggerhoff *et al.* 2001). Here we report new temperature measurements performed at the rock–atmosphere interface in the Aburatsubo underground observatory.

THE SITE AND THE EXPERIMENTAL SET-UP

The temperature measurements were performed in the vault of the Aburatsubo observatory where resistivity measurements have been performed since 1977 (Fig. 1). The host rock is a weakly consolidated tuff formation with a porosity Φ of the order of 40 per cent and a volume water saturation S_w of the order of 85 per cent (Utada *et al.* 1998). The cavity has a height h of about 2 m and a floor surface area S of 68 m^2 (Fig. 2). It is located about 2 m above an aquifer connected to the sea, as revealed by resistivity soundings (Yoshino *et al.* 1998).

The room is protected from external ventilation by a set of doors (Fig. 2) and is subject to temperature changes associated with diffusion from the ground surface through about 6 m of rock, and possibly to water percolation associated with rainfall. Nevertheless, no open fractures or water inflow are observed in the cavity. Pressure variations can in principle also induce temperature changes and water transport (Pisarenko *et al.* 1996; Perrier *et al.* 2001). The average temperature of the atmosphere is 17.5 °C.

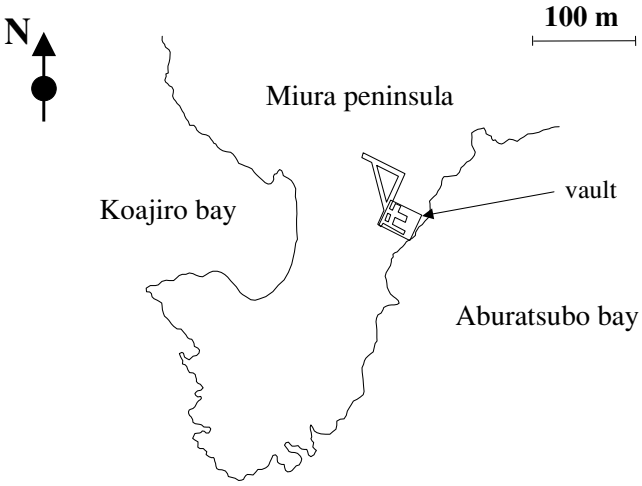

Figure 1. Map of the Miura peninsula (about 60 km southwest of Tokyo) showing the location of the Aburatsubo experimental vault.

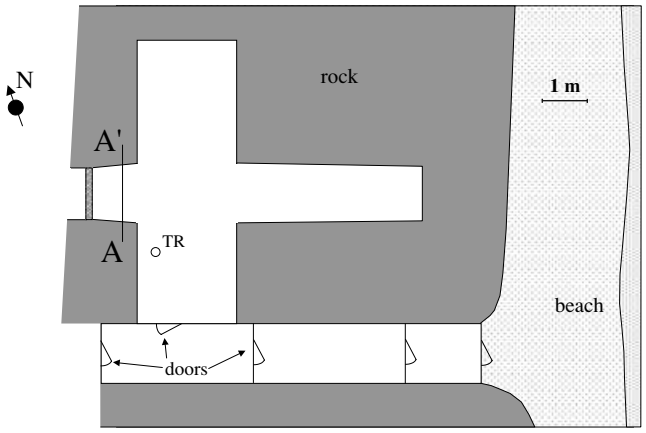

Figure 2. Layout of the underground vault used for resistivity measurements since 1977. The point TR indicates the location of temperature measurements performed at various depth intervals in the rock (Yoshino *et al.* 1998). AA′ indicates the location of the cross-section shown in Fig. 3.

The temperature measurements were performed about 1 m from a cement wall closing the access to another room where ground tilt and extension were measured (Fig. 2). Ten thermistors, labelled TA1 to TA10, were installed at a depth of about 2 cm in the rock with a spacing of about 40 cm (Fig. 3). Each thermistor has a length of 30 mm and a diameter of 5 mm, and is characterized by a relationship between resistance and temperature given approximately by:

$$R = R_0 e^{-T/T_0}, \quad (1)$$

where R is the resistance, T the temperature in degrees Celsius, and R_0 and T_0 are constants with values of 5800 Ω and 23 °C respectively, leading to a sensitivity of about 118 Ω °C^{-1} at 17.5 °C. Data are recorded with a sampling interval varying from 1 to 5 min.

The absolute calibration of the thermistors is not known to better than 0.2 °C but, for this experiment, a careful relative calibration

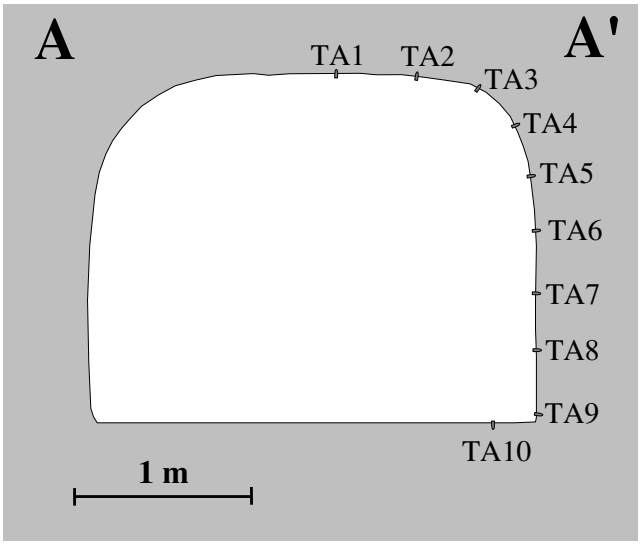

Figure 3. Position of the 10 thermistors used in the present study. The position of this cross-section is indicated in Fig. 2.

was performed. For this purpose, the 10 sensors were monitored in a regulated and stirred thermal bath for several hours. A linear relationship between the resistance values of TA2 to TA10 as a function of the resistance of TA1 taken as reference was observed and fitted. The results of these fits were then used to correct the observed resistance values measured in the cavity before the global absolute conversion function given by eq. (1) was applied. The expected precision of this relative calibration is of the order of 0.005 °C.

OVERVIEW OF THE TEMPERATURE PROFILE DATA

The vertical temperature profile has been operating since 2000 September without interruption except for a few minutes at the time of the monthly maintenance (Fig. 4). The data exhibit a yearly variation of about 1.2 °C peak to peak, in agreement with previous measurements in the ground (Utada *et al.* 1998; Yoshino *et al.* 1998), on top of a temperature increase of about 0.1 °C per year. The most striking feature of the data (Fig. 4) is that temperatures at TA9 and TA10 are significantly lower than the other eight temperatures from May to October, in a reproducible manner, whereas during the period from November to April, temperatures TA7 to TA10 vary grouped together with lower values, separated from TA1 to TA6 at higher values.

In Fig. 5(a) the average temperature is shown as a function of time and it is compared with an annual sinusoidal variation of amplitude 0.6 °C on top of a linear trend of 0.1 °C per year. The curve describes the data well, except during the year 2002 during which larger perturbations have been taking place. In 2002 March, indeed, extensive work took place in the cavity and seems to have perturbed the annual cycle for the remainder of the data set.

Before 2002, the residuals, defined as the difference between the data and the curve, remain smaller than 0.1 °C. These variations are coherent over the 10 sensors (Fig. 4). Some coherent transient variations of about 1 month's duration, for example in 2001 May and June, could be correlated with the rainfall recorded at the Miura weather station located 3 km northeast of Aburatsubo (Fig. 5b), but no systematic pattern emerges between the transient temperature variations and rainfall. Note in particular that although positive temperature variations tend to follow the large rain spikes in 2001 August and September, another similar temperature variation is observed in 2001 July, when no significant rainfall was recorded. Spikes and short-term changes also emerge in Figs 4 and 5: they are associated with human presence in the cavity. Such artificial perturbations actually provide useful and important information, as discussed later.

The vertical temperature difference $T_{\text{ceiling}} - T_{\text{floor}}$ is also shown as a function of time in Fig. 5(c). The ceiling temperature T_{ceiling} is defined as the average value of TA1, TA2 and TA3 which are installed in the roughly horizontal ceiling (Fig. 3). The floor temperature T_{floor} is defined as the average of TA9 and TA10. The vertical temperature difference always remains positive, with values varying with time from 0.04 to 0.28 °C, with a clear semi-annual seasonal pattern. Moreover, this positive difference is gradually increasing with time

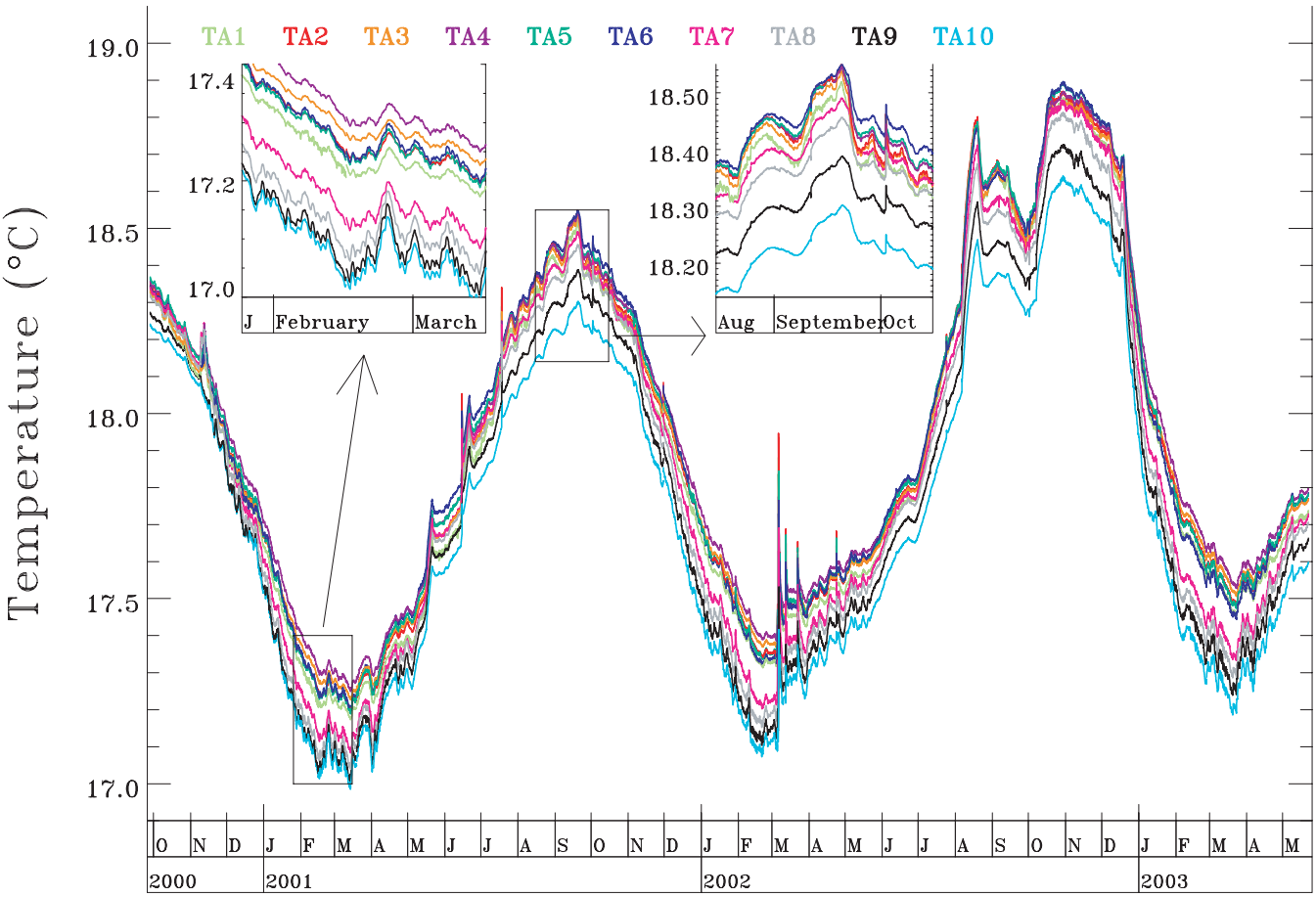

Figure 4. Hourly averages of the 10 temperature sensors as a function of time.

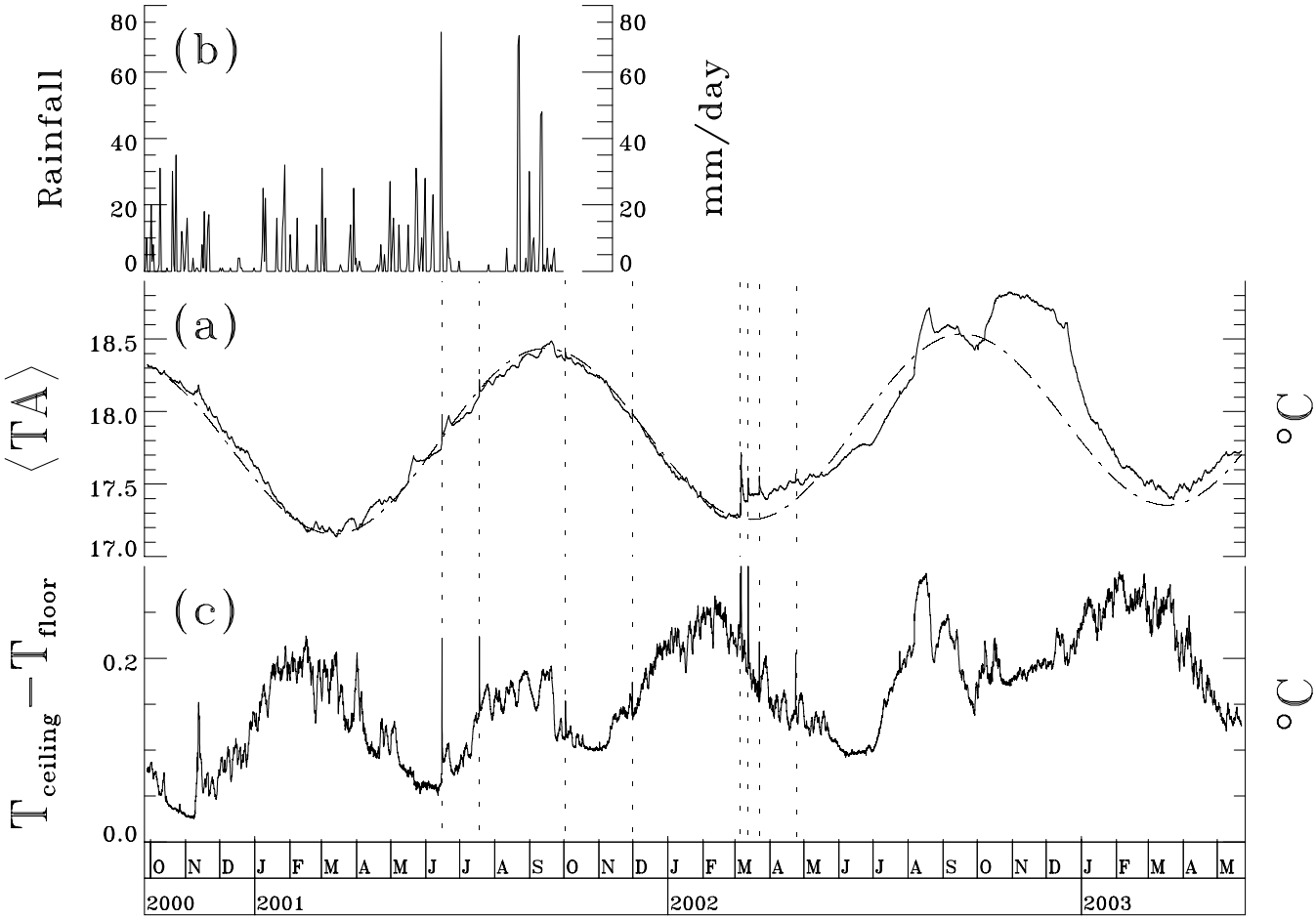

Figure 5. Presented as a function of time: (a) average value of the 10 temperatures compared with a sinusoidal annual wave of amplitude 1.2 °C plus a linear increase of 0.1 °C per year; (b) rainfall record from the Miura meteorological station located 3 km northeast of Aburatsubo; (c) the vertical temperature gradient taking the average of TA1, TA2 and TA3 (Fig. 2) as the ceiling temperature and the average of TA9 and TA10 as the floor temperature. The vertical dotted lines indicate human presence in the vault.

(Fig. 5c). In addition, from May to October (summer regime), the temperature difference is characterized by transients with a period of about 2 weeks to 1 month. From November to April (winter regime) these transients are dominated by higher-frequency variations of a more oscillatory type.

The average vertical residual temperature profile is shown in Fig. 6 separately for various time intervals. As was already shown in Figs 4 and 5, the temperature of the ceiling is higher than the temperature of the floor. In addition, a smooth spatial variation is observed. The maximum temperature may not be at the ceiling but at the top region of the wall between sensors TA4 and TA5 (Fig. 3). However, to a first-order approximation, the temperature can be considered spatially uniform over the ceiling and the upper part of the wall, with a fast linear decrease of temperature from about half height to the floor. The profiles for the winter and summer regimes are slightly different, but both are reproducible from year to year to an astonishing degree of precision, even for the last profiles of 2002, although they are shifted because of the perturbation mentioned earlier. In particular, the curvature of the spatial temperature variation for sensors TA7 to TA10 is convex for the summer regimes and concave for the winter regimes.

Note that the relative calibration of the sensors is essential to obtain the smooth and reproducible profiles of Fig. 6. If a smooth polynomial of degree 3 is fitted to the spatial variations shown in Fig. 6, the standard deviation of the difference between the observed temperature and the polynomial is about 0.013 °C on average. This provides an estimate of the relative temperature calibration error of the sensors. If the relative calibration is not taken into account, no smooth profile is observed and this standard deviation is increased to 0.070 °C. Without the relative calibration, the resolution would have been insufficient to guarantee that the ceiling temperature is systematically higher than the floor temperature. Note, however, that if the relative calibration is not taken into account a linear fit of the temperature as a function of position still would have led to a positive slope, and hence suggested a vertical positive gradient, but with a much reduced significance.

RESPONSE OF THE TEMPERATURE PROFILE TO PERTURBATIONS

The coherent transient temperature variations, if not associated with rainfall as mentioned earlier, could be related to variations of atmospheric pressure (Perrier *et al.* 2001). Temperature variations ranging (1-40) $\times 10^{-3}$ °C $(\mathrm{hPa})^{-1}$ have been observed in the atmosphere of an underground limestone quarry in Vincennes, near Paris, France (Perrier *et al.* 2001). In Aburatsubo, most coherent transient temperature variations are of the order of 0.1 °C (Figs 4 and 7) and are

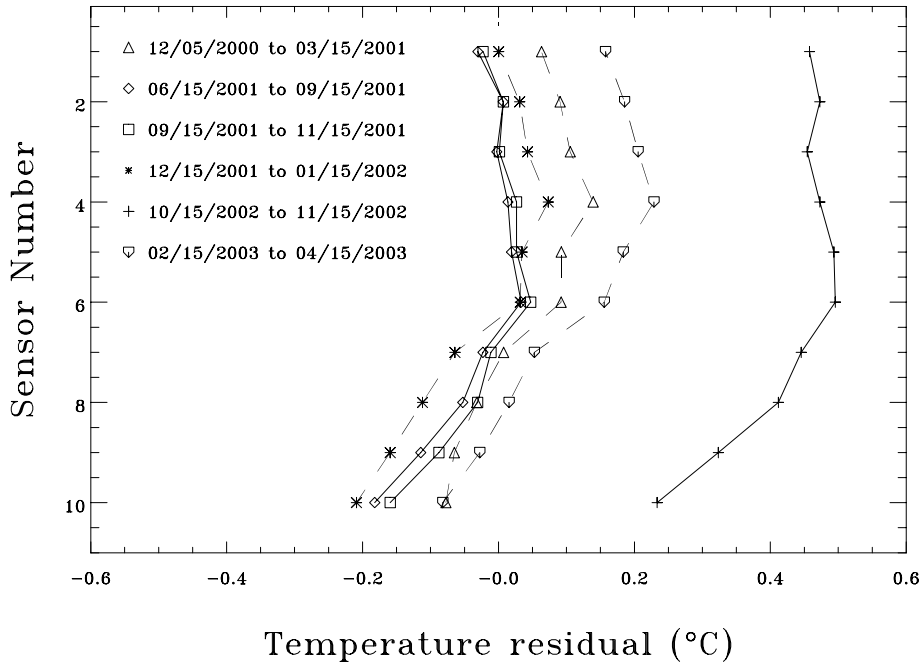

Figure 6. Vertical profile obtained from the thermistor set-up (Fig. 3). Time averages obtained over several periods are compared.

therefore too large to be attributed to pressure variations, except for abrupt changes during typhoons. The effects of two typhoons for example (typhoon number 15 and typhoon number 11) are visible in Fig. 7. The corresponding temperature disturbances depend on the position in the cavity as shown in Fig. 8(a). The maximum value amounts to 25×10^{-3} °C for typhoon number 15 and 9×10^{-3} °C for typhoon number 11, corresponding respectively to couplings of 0.9×10^{-3} and 0.75×10^{-3} °C $(\mathrm{hPa})^{-1}$, in agreement with the Vincennes experiment. Note that a characteristic spatial structure of the response emerges in Fig. 8(a), reproducible for the two typhoons. This spatial structure is not present in the average temperature profiles of Fig. 6, and thus must be due to a local effect that can affect the short-term response (periods of the order of 1 hr), but not long-term variations with periods longer than 1 day.

In addition to natural disturbances such as typhoons, our temperature profile data are also perturbed by human presence (Figs 4, 5 and 7). The thermal effect of human presence is visible for several hours after the cavity has been isolated again and the time necessary to recover from the perturbation is more than 2 days. Assuming a constant exponential decay, a characteristic time of the order of 30 hr is obtained for all sensor positions.

The amplitude of two perturbations is shown as a function of position in Fig. 8(b). Amplitudes vary from 0.05 to 0.2 °C, significantly larger than the response to typhoons. The response to human presence has a definite spatial variation, with a maximum in the middle of the ceiling (sensor TA1). Each human presence, at rest, provides a local thermal buoyancy source with a power of the order of 100 to 140 W (e.g. Villar *et al.* 1984; Linden 1999). The heating then results in the formation of a layer of hot air that progressively invades the cavity from the top with a filling box mechanism (Baines & Turner 1969). The amplitude of the heating (0.2 °C) is compatible with the results of heating experiments performed in the Vincennes quarry (Crouzeix *et al.* 2003) and measurements performed in painted caves during visits (Hoyos *et al.* 1998; Sanchez-Moral *et al.* 1999).

CHARACTERIZATION OF THE SUMMER AND WINTER THERMAL REGIMES

Summer and winter regimes can also be characterised as follows. The relative amplitude of the coherent temperature waves TA*i* with respect to TA1 is estimated by a simple correlation ratio :

$$\mathrm{TA}i/\mathrm{TA1} = \frac{\sum_k \mathrm{TA}i(k)\mathrm{TA1}(k)}{\sqrt{\sum_k \mathrm{TA1}(k)^2}}, \qquad (2)$$

where TA$i(k)$ refers to a given temperature residual time series for sensor TA*i* and TA1(k) the corresponding time series for sensor TA1. This correlation ratio is calculated by averaging the values obtained from four consecutive time intervals of a duration of 4 days each. The ratios TA10/TA1 and TA6/TA1 are shown as a function of time in Fig. 9 and all ratios TA*i*/TA1 are shown as a function of position in Fig. 10(a). These ratios exhibit seasonal variations that precisely correspond to the previously defined summer and winter regimes (Fig. 9). During winter regimes, the coherent temperature variations have amplitudes about two times larger on the floor compared with the ceiling, and, during summer regime, amplitudes about two times smaller on the floor compared with the ceiling. This fact could actually already be noticed in Fig. 4. This time and spatial structure is reproducible as indicated by Fig. 9, and by the overlap of the two winter and summer profiles of ratios shown in Fig. 10(a). Not only is the magnitude of the ratios reproducible, but also their spatial structure to the finest details. Moreover, the perturbation of 2002 March does not affect this pattern.

The frequency contents of the temperature residual of sensor TA10 during the winter and summer regimes are compared in Fig. 11. Both temperature power spectra are dominated by a f^{-2} variation, where f is the frequency, over more than two orders of magnitude of frequency. This spectral exponent indicates a signal typical of Brownian noise (e.g. Turcotte 1992). In the case of the

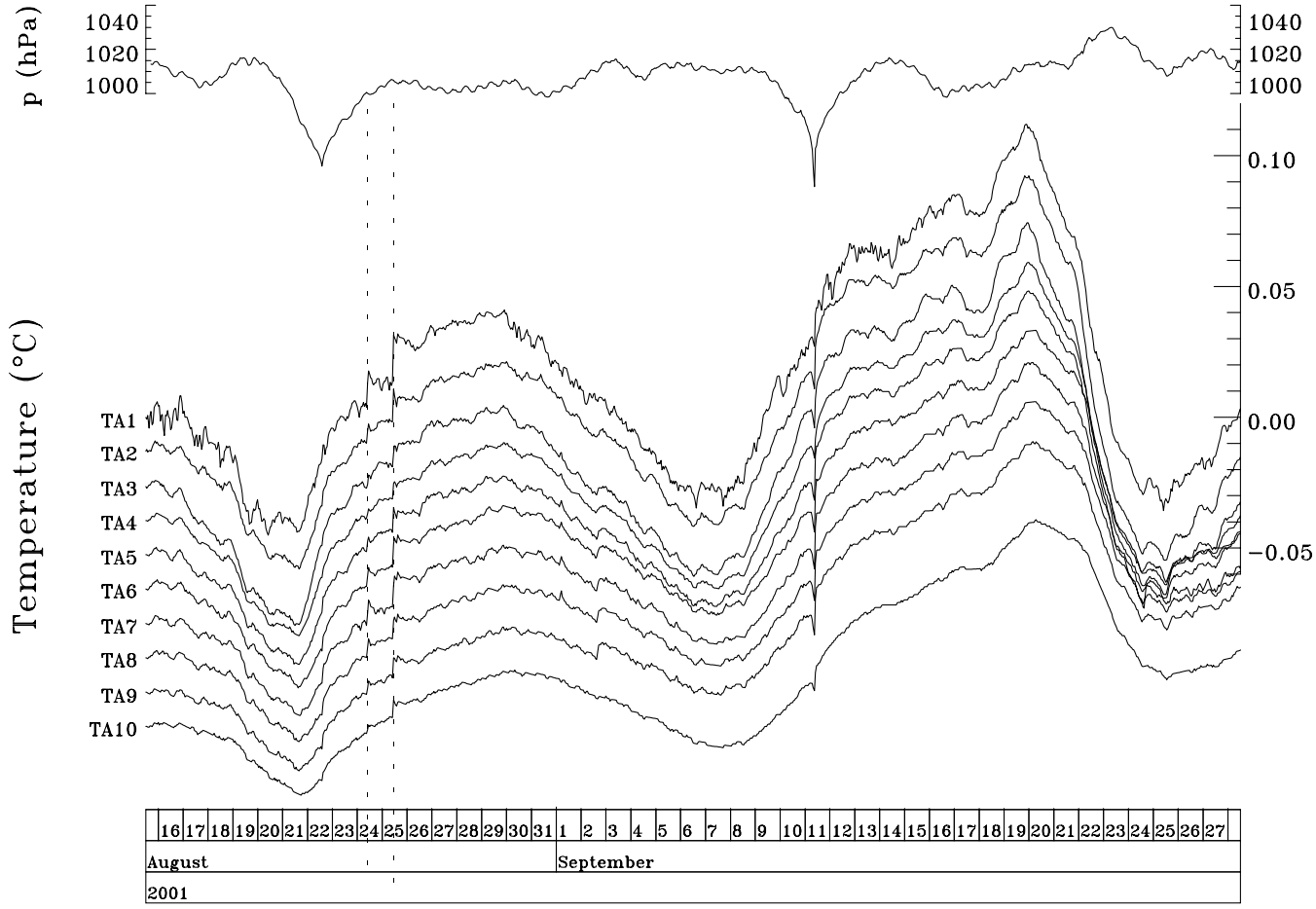

Figure 7. Atmospheric pressure and temperatures as a function of time. The vertical dotted lines indicate human presence in the vault. The two pressure minima correspond to typhoon number 11 (2001 August 22) and typhoon number 15 (2001 September 11).

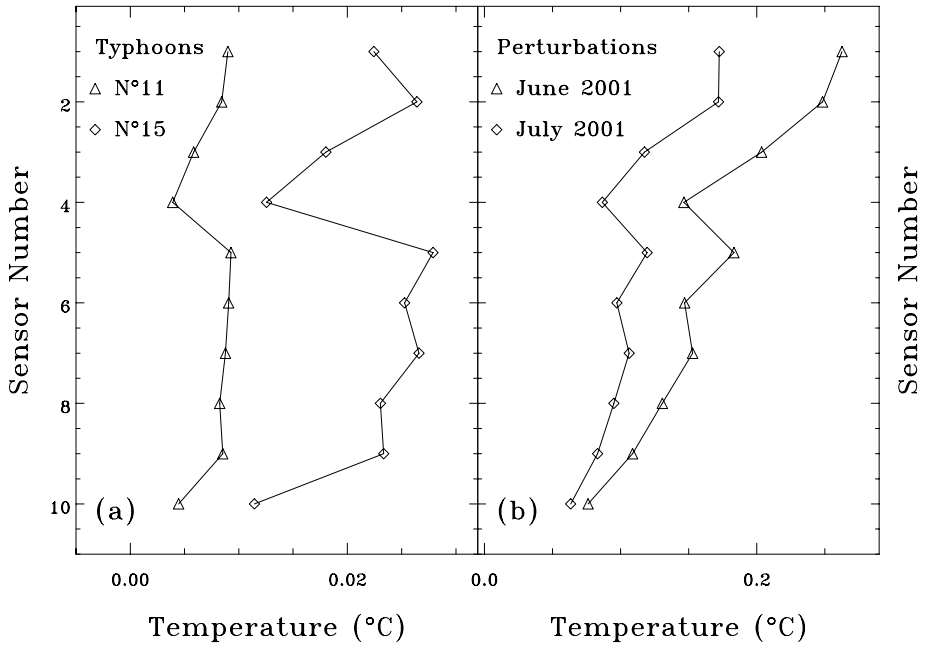

Figure 8. Spatial variation of the peak temperature response to typhoons (a) and perturbations associated with human presence (b).

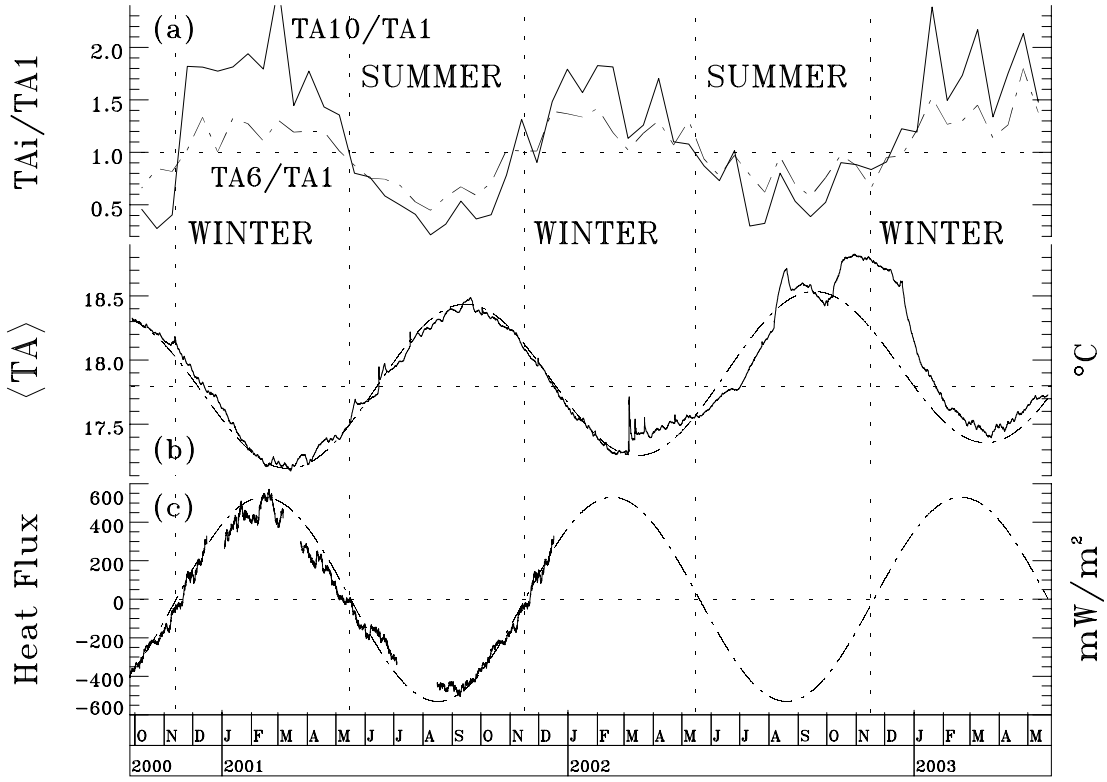

Figure 9. Presented as a function of time: (a) detrended amplitude ratio TA10/TA1 and TA6/TA1 obtained over 16 day-long sections of hourly averages; (b) average value of the 10 temperatures compared with a sine annual wave of amplitude 1.2 °C plus a linear increase of 0.1 °C per year; (c) heat flux at floor level determined from temperature records in 1999 obtained at 34 cm and 66 cm at point TR. The line corresponds to the heat flux at floor level associated with the sine wave depicted in (b).

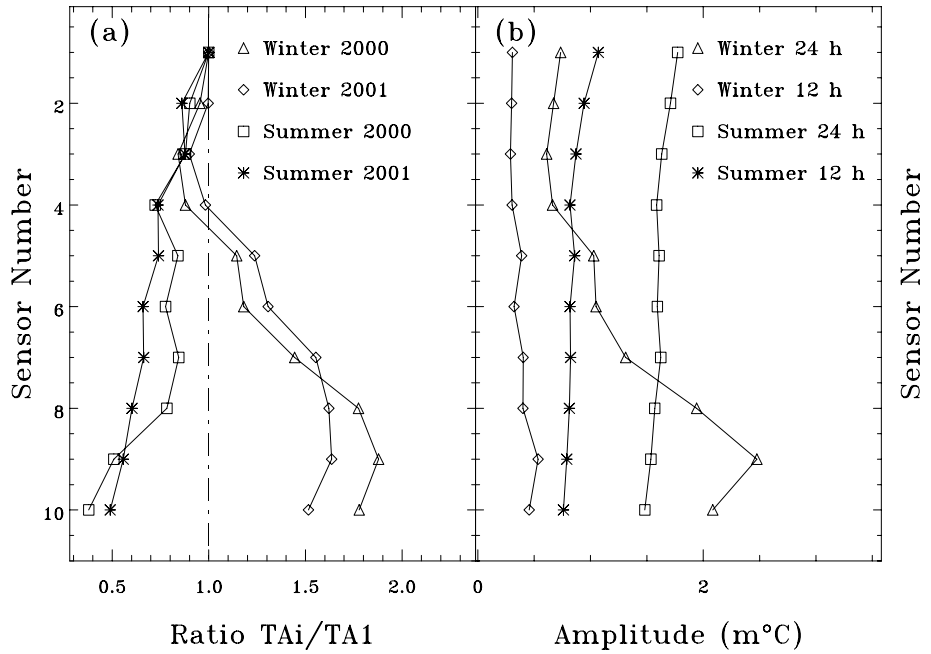

Figure 10. As a function of sensor position: (a) amplitude correlation ratios obtained over 16-day sections; (b) amplitudes of 24 hr and 12 hr spectral lines.

winter spectrum, two lines corresponding to the 24 hr and 12 hr variations are clearly visible.

The magnitude of the 24 hr and 12 hr lines is shown in Fig. 10(b) as a function of position. During summer, the spectral lines are characterized by a slowly increasing intensity as a function of position in the cavity. During winter, however, a strong increase of the 24-hr line is observed for the lower sensors TA8 to TA10. The shape of this variation is in agreement with the spatial pattern of variation

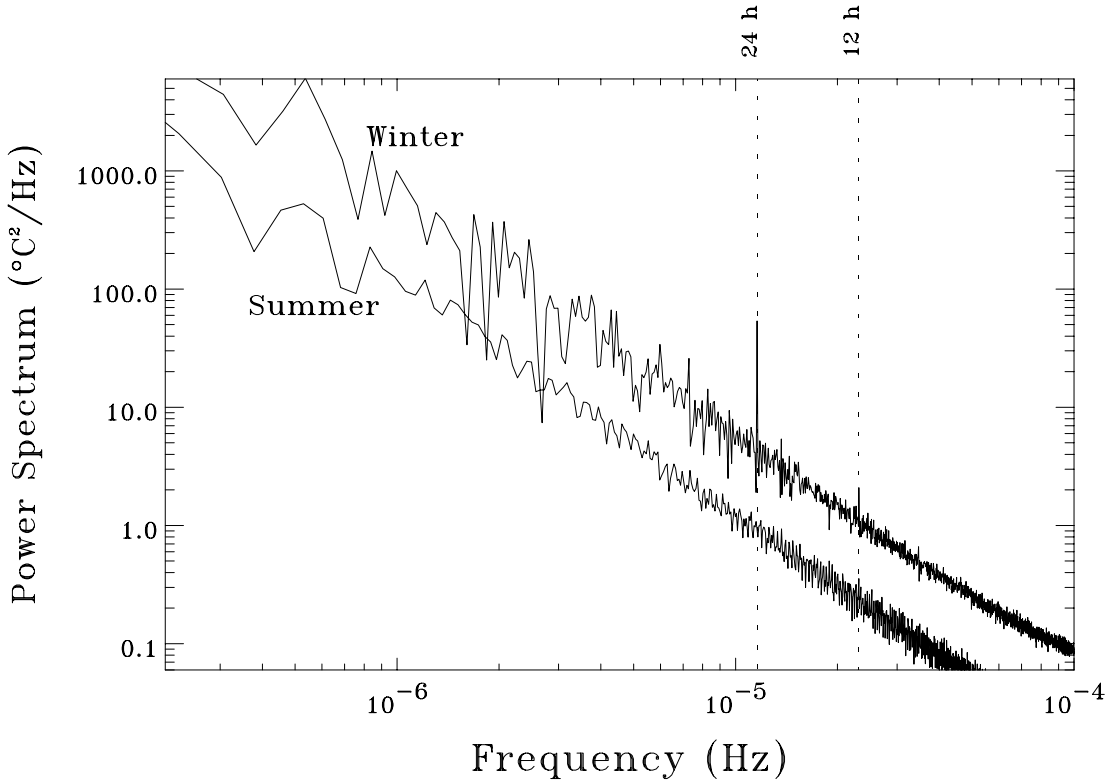

Figure 11. Power density spectrum of sensor TA10 temperature residual obtained from 2000 November 30 to 2001 April 30 (winter) and from 2001 May 15 to 2001 October 15 (summer). The summer spectrum has been shifted down by a factor of 10 for clarity.

of the correlation factors in winter of Fig. 10(a), indicating that the maximum amplitudes occur at sensor TA9.

The correlation of the various sensors to TA1, calculated so far in the time domain, can also be studied in the frequency domain (Fig. 12). The coherence is calculated as the modulus of correlation obtained from four consecutive time sections. In summer, the modulus of the transfer functions TA10/TA1, TA6/TA1 and TA3/TA1 is smaller than one over the whole frequency range, in agreement with the previous results given by the correlation ratios (eq. 2), with the additional information of a negative phase (phase delay). The coherence is above 0.8 and a possible slight frequency variation is suggested by the data. During winter, however, the pattern is more complicated than anticipated from the time domain correlation ratios. The modulus is decreasing significantly, from values larger than 1 at the lower frequencies, associated with increasing and positive phases (phase advance) and a significantly decreasing coherence at periods of a few hours.

To conclude, an amazingly coherent picture emerges from the temperature profile data. All transient and oscillatory variations are spatially organized according to the two regimes. This remarkable organization suggests that the transient thermal perturbations are likely to have little relationship to meteorological artefacts such as rainfall but rather are signatures of physical processes in the cavity itself.

INTERPRETATION IN TERMS OF HEAT FLUX

The transition between the summer and winter regimes occurs about one and a half months after the temperature maximum (Figs 4 and 5), corresponding to about one-eighth of a period. For any 1-D harmonic diffusion process, this corresponds to the time of change of sign of the flux. Indeed, consider a 1-D thermal diffusion along a vertical axis z (positive upwards) in a medium of thermal conductivity K_T and thermal diffusivity $\kappa (\kappa = K_\mathrm{T}/\rho_\mathrm{r} c_\mathrm{p}$ where ρ_r is the density and c_p the specific heat). The temperature T is given as a function of position and time t by:

$$T(z,t) = \cos\left(2\pi\frac{t}{t_0} + \frac{z}{\lambda_\mathrm{T}}\right) \mathrm{e}^{z/\lambda_\mathrm{T}}, \tag{3}$$

where t_0 is the period and λ_T is the thermal diffusion length $\sqrt{\kappa t_0/\pi}$, assuming a variation normalized to ± 1 at $z = 0$. The heat flux F is then given by

$$\begin{aligned} F(z,t) &= -K_\mathrm{T}\frac{\partial T}{\partial z} \\ &= -\frac{K_\mathrm{T}\sqrt{2}}{\lambda_\mathrm{T}} \cos\left(2\pi\frac{t}{t_0} + \frac{z}{\lambda_\mathrm{T}} + \frac{\pi}{4}\right) \mathrm{e}^{z/\lambda_\mathrm{T}}, \end{aligned} \tag{4}$$

which is crossing zero from negative to positive values when $t = t_0/8$ at $z = 0$.

This suggests that the heat flux is upward during the winter regime from November to April and downward during the summer regime from May to October. This guess can be confirmed because a restricted set of temperature measurements is available in the vault (point TR in Fig. 2) at various depth intervals: 2, 34, 50, 66 and 98 cm (Utada *et al.* 1998; Yoshino *et al.* 1998, Fig. 10). An estimate of the heat flux in the rock below the cavity can then be obtained from

$$F_{ij} = -K_\mathrm{T}\frac{T_i - T_j}{z_i - z_j}, \tag{5}$$

where T_i and T_j are the temperatures measured at depths i and j respectively. The heat flux given by eq. (5) is an estimate at the

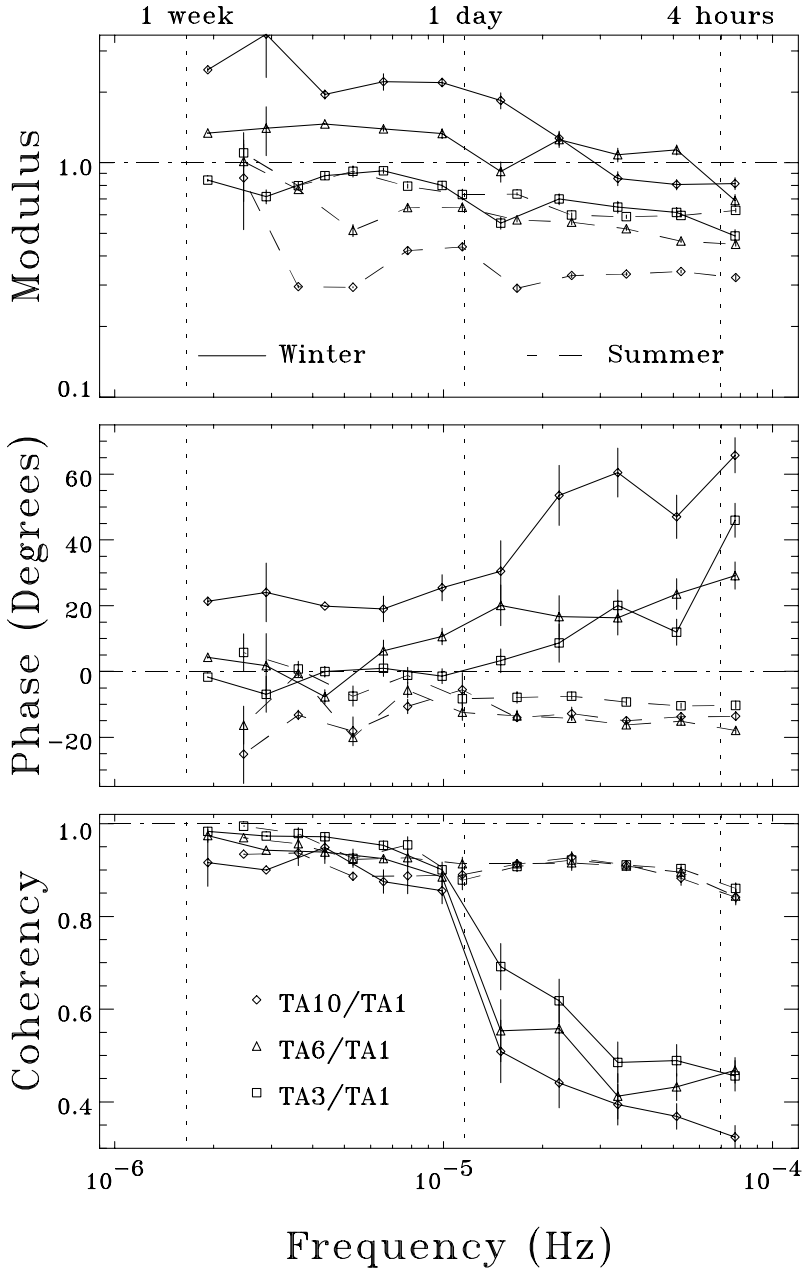

Figure 12. Modulus, phase and coherence as function of frequency of the transfer function of temperature TA10, TA6 and TA3 with respect to TA1. The winter subsection corresponds to 2000 December 1 to 2001 April 1 and the summer subsection corresponds to 2001 July 1 to 2001 November 1. The transfer function is computed using 15-day-long sections of hourly averages of temperature residuals.

average depth $1/2(z_i + z_j)$, but can be transferred to a reference level at the floor of the cavity using eq. (4). In the cavity itself, the heat transfer may not be conductive; then eq. (3) cannot be applied. Indeed, the data show (Fig. 4) that the annual temperatures variations are in phase from ceiling to floor.

In Fig. 9, the heat flux at the floor of the cavity obtained from the temperature measurements at depths of 34 and 66 cm is compared with the simple 1-D expectation given by eq. (4) derived from the average values of the TA sensors. A value of $K_T = 2$ W m^{-1} K^{-1} is used for the thermal conductivity of the rock (Musy & Soutter 1991), compatible with the measured value for wet tuff at Yucca Mountain (Birkholzer & Tsang 2000). The thermal diffusion length for the annual variation is taken as 3.2 m, corresponding to a thermal diffusivity κ of 10^{-6} m^2 s^{-1} (Utada *et al.* 1998). The heat flux data were obtained mostly in 1999 and they are therefore artificially shifted by 1 yr and 2 yr to the 2000 September to 2002 January period. The amplitude and, more significantly, the phase are in good agreement with the expectation and support the hypothesis that the winter and summer regimes are driven by the direction of the heat flux in the cavity. The measured peak magnitude of the heat flux amounts to 0.4 W m^{-2}, which is slightly smaller than the expected magnitude. The difference is, however, not significant given the simplicity of the calculation and the artificial 1-yr time shifts. In addition, given the fact that the pattern of heat flux through and around the cavity is actually at least 2-D, a larger discrepancy between the data and the simple estimate would still have been acceptable.

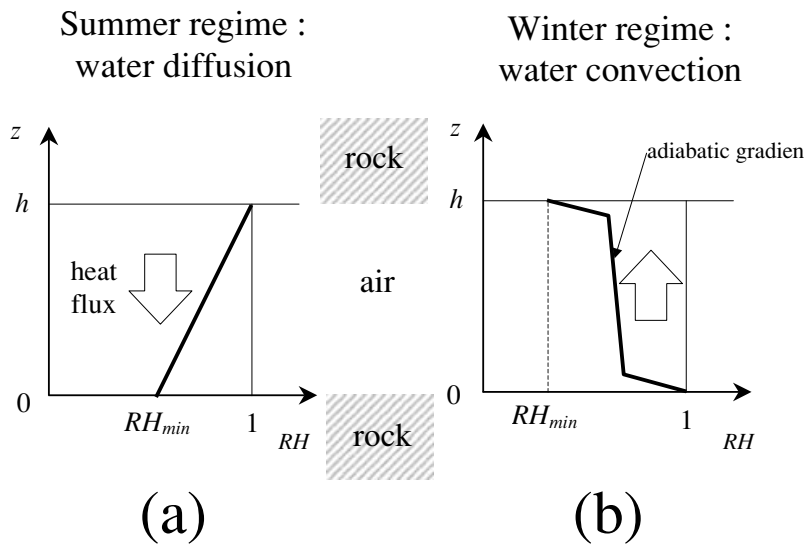

Figure 13. Sketch of the vertical relative humidity distribution in a cavity in the presence of a downward heat flux (a) or an upward heat flux (b).

Both the heat flux at the floor of the cavity and the vertical temperature profile are measured quantities and the details of the heat transfer from the ground surface into the large scale embedding of the cavity are therefore not essential. In particular, the effects of the topography, rock heterogeneity, ocean or the aquifer need not be considered. Here, we have to address how, given the boundary conditions, the heat transfer takes place locally through the air of the cavity.

ESTIMATES OF HEAT TRANSFER MECHANISMS THROUGH THE CAVITY

The Aburatsubo vault is characterized by two important facts: the ceiling temperature is always higher than the floor temperature (Fig. 5c) and the cavity is subject to a large seasonal heat flux of peak magnitude $\pm 400 \times 10^{-3}$ W m^{-2} (Fig. 9c); this is large compared with the geothermal heat flow which is measured to amount to 30×10^{-3} W m^{-2} at Yokosuka, in the Miura peninsula, 15 km northeast of Aburatsubo. Since the ceiling temperature is always larger than the floor temperature, thermal convection cannot take place. The heat flux $F_{\mathrm{T}}^{\mathrm{D}}$ by thermal diffusion in the cavity atmosphere is always downward and its value is given by:

$$F_{\mathrm{T}}^{\mathrm{D}} = -K_{\mathrm{T}}^{\mathrm{a}} \frac{T_{\mathrm{roof}} - T_{\mathrm{floor}}}{h}, \tag{6}$$

where $K_{\mathrm{T}}^{\mathrm{a}}$ is the thermal conductivity of dry air. Taking $K_{\mathrm{T}}^{\mathrm{a}} = 0.023$ W^{-1} m^{-1} K^{-1} (Musy & Soutter 1991), this expression gives a maximal value of -2.3×10^{-3} W m^{-2}, which is negligible.

Radiative transfer, however, can be an important contribution to heat transfer in underground cavities (Villar *et al.* 1984). In our case, the vertical radiative heat flux $F_{\mathrm{T}}^{\mathrm{R}}$ can be estimated as (Villar *et al.* 1984):

$$F_{\mathrm{T}}^{\mathrm{R}} = -\sigma \varepsilon_{\mathrm{c}} T_0^3 \left(T_{\mathrm{roof}} - T_{\mathrm{floor}}\right), \tag{7}$$

where T_0 is the average absolute temperature in the cavity (290 K), σ is the Stefan constant (5.67×10^{-8} W m^{-2} K^{-4}) and ε_{c} is an emissivity constant depending on the amount of water vapour and CO_2 in the cavity. Taking $\varepsilon_{\mathrm{c}} = 0.8$ (Villar *et al.* 1984), the radiative heat flux is always negative, with a peak value of -220×10^{-3} W m^{-2}, which is significant compared with the maximum seasonal heat flux of $\pm 400 \times 10^{-3}$ W m^{-2}.

Since the vertical temperature gradient is locked to positive values, the time-varying heat flux through the cavity must be transferred through phase changes of water. The heat flux to be transferred by water vapour (F_{w}) is given by $F - F_{\mathrm{T}}^{\mathrm{R}}$ and has a peak value of 620×10^{-3} W m^{-2} in winter (positive, upwards) and -180×10^{-3} W m^{-2} (negative, downwards) in summer, with the above estimates.

In summer (Fig. 13a), water vapour can transport heat downwards by evaporation on the ceiling and condensation on the floor, and the transport in the atmosphere of the cavity can take place by diffusion of water vapour. Indeed, if a linear profile of relative humidity exists in the cavity as depicted in Fig. 13(a), then the heat flux $F_{\mathrm{w}}^{\mathrm{D}}$ transferred by water diffusion is given by:

$$F_{\mathrm{w}}^{\mathrm{D}} = -L D c_{\mathrm{w}}^{\mathrm{s}} \frac{RH_{\max} - RH_{\min}}{h}, \tag{8}$$

where L is the latent heat of vaporization of water (2.5×10^6 J kg^{-1}), D is the diffusion coefficient of water in air (2.1×10^{-5} m^2 s^{-1}), $c_{\mathrm{w}}^{\mathrm{s}}$ is the saturated water content of air at 17.5 °C (0.0152 kg m^{-3}) and $RH_{\max}$ and $RH_{\min}$ define the range of relative humidity variation in the cavity (Fig. 13a). Taking $RH_{\max} = 1$ and $RH_{\min} = 0.4$, eq. (8) gives -240×10^{-3} W m^{-2}. Water diffusion can therefore accommodate the required heat flux during summer. Note that if radiative transfers are not taken into account, the maximum heat flux that can be accounted for by water vapour diffusion corresponds to $RH_{\min} = 0$ and amounts to -398×10^{-3} W m^{-2}.

In winter, the direction of heat flux to be transferred by water is reversed and the water-saturated layer of air must be at floor level. This configuration is unstable and leads to a strong buoyant convection regime (Fig. 13b). When convection is established, the relative humidity profile will be almost homogeneous in the cavity, with at most a small adiabatic gradient, with diffusive transfer in the boundary layers only. The presence of convection in winter is also compatible with transient variations with shorter timescales compared with the summer regime, and a phase advance at the floor with respect to the ceiling.

Known scaling relations of turbulent convection can be used to estimate the convective heat flux $F_{\mathrm{w}}^{\mathrm{C}}$ transferred by the water vapour buoyancy, expressed as (e.g. Grossmann & Lohse 2000, 2001):

$$F_{\rm w}^{\rm C} = NuF_{\rm w}^{\rm D}, \tag{9}$$

where the diffusive heat flux $F_{\rm w}^{\rm D}$ is given by eq. (8) and Nu is the Nusselt number, related to the Rayleigh number Ra by a universal scaling relation:

$$Nu = cRa^{\alpha}, \tag{10}$$

with $c = 0.22$ and $\alpha = 0.29$. Here Ra is defined as:

$$Ra = \frac{Bh^3}{\nu D}, \tag{11}$$

where ν is the kinematic viscosity of air (1.6×10^{-5} m^2 s^{-1}) and B is the buoyancy given by

$$B = g\frac{\Delta\rho_{\rm a}}{\rho_{\rm a}^{\rm d}} = g(RH_{\max} - RH_{\min})\frac{p_{\rm v}}{p}\frac{M_{\rm a} - M_{\rm w}}{M_{\rm a}}, \tag{12}$$

where g is the acceleration of gravity, $\rho_{\rm a}^{\rm d}$ the density of dry air, $\Delta\rho_{\rm a}$ the density difference due to water vapour, $p_{\rm v}$ the saturated vapour pressure (2048 Pa at 17.5 °C), p the atmospheric pressure, $M_{\rm a}$ the molar mass of dry air (0.029 kg) and $M_{\rm w}$ the molar mass of water (0.018 kg). Assuming, as an example, $RH_{\max} = 1$ and $RH_{\min} = 0.96$, one has $Ra = 7.2 \times 10^7$, a value well in the turbulent convection regime, which gives $Nu = 42$ according to eq. (10). According to eqs (8) and (9), the heat flux then amounts to 670×10^{-3} W m^{-2}. In the convective regime, even with a small vertical relative humidity gradient, the necessary upward heat flux can be accommodated. The thickness of the thermal boundary layer can be estimated as $0.5h/Nu$ (e.g. Grossmann & Lohse 2000) and has a value of the order of 2 cm.

Conversely, from eqs (8) to (12), in the context of the simple models depicted in Fig. 13, the relative humidity profile in the cavity can also be expressed as a function of time (Fig. 14). The contribution of the radiative heat transfer is calculated as a function of time using eq. (7) and an approximated smooth variation as a function of time of the temperature difference $T_{\rm ceiling} - T_{\rm floor}$, adjusted to the measured values shown in Fig. 5(c). The predicted relative humidities at ceiling level, floor level and at mid-height are shown in Fig. 14(b). During the winter regime (upward heat flux), the reduction of saturation of the atmosphere is at most 4 per cent at ceiling level, which is difficult to measure. To a first approximation, the atmosphere thus remains close to saturation during the whole winter regime. During the summer regime, however, a significant, and in principle measurable, desaturation of the atmosphere is expected from July to September, especially at floor level where a relative humidity of 40 per cent is possible. This estimate, however, relies on the knowledge of the radiative heat transfer, which accounts for about half of the heat flux, and which remains rather uncertain.

ESTIMATES OF SEASONAL LIQUID WATER FLOW

The liquid water volume flow rate $Q_{\rm w}$ necessary to account for the heat flux is given by $F_{\rm w}/L\rho_{\rm w}$ where $\rho_{\rm w}$ is the density of liquid water, and is also shown in Fig 14(c) as a function of time. Maximum values of the order of 1 ml m^{-2} hr^{-1} are calculated for the condensation rate on the ceiling in winter. Because of the contribution of radiative heat transfer, a smaller maximum value of -0.3 ml m^{-2} hr^{-1} is expected for the condensation rate on the floor in summer. This small water flow changes the average saturation $S_{\rm w}$ of the rock mass below the cavity according to

$$\frac{dS_{\rm w}}{dt} = -\frac{Q_{\rm w}}{\Phi d_{\rm R}}, \tag{13}$$

where $d_{\rm R}$ is the thickness of the affected rock layer and Φ is the total porosity (40 per cent). Taking $d_{\rm R} = 40$ cm, which is a reasonable value as the depth of the aquifer is about 2 m (Yoshino *et al.* 1998), the resulting saturation change $\Delta S_{\rm w}$ is shown in Fig. 14(c) as a function of time. An annual variation of the order of 1 per cent is observed but, in addition, as the water flow is not symmetrical because of the permanent downward contribution of radiative transfer to the heat flux, a net desaturation of the rock mass of the same

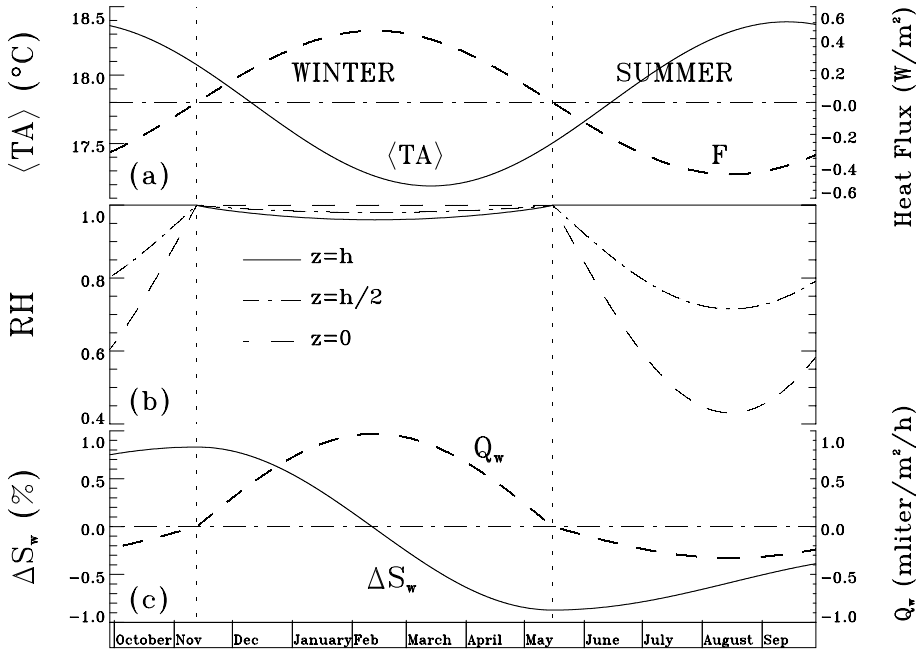

Figure 14. Presented as a function of time: (a) the mean average temperature of the rock (left scale) and the associated heat flux (right scale); (b) the relative humidity of the atmosphere of the cavity at floor, ceiling and intermediate level; (c) the saturation change $\Delta S_{\rm w}$ (left scale) of a layer of 40 cm of rocks below the cavity associated with the water flow $Q_{\rm w}$ (right scale) inferred from the total heat flux depicted in (a), taking into account the radiative contribution.

order of magnitude is expected to take place simultaneously. This effect may contribute to the observed steady increase of resistivity as a function of time (Utada *et al.* 1998).

Concerning the co-seismic resistivity changes, the fact that the annual cycle of the sign of the resistivity changes corresponds to the sign of the heat flux (Utada *et al.* 1998) is now clarified. Indeed, in our model, heat flux is related to water flow, and thus can drive the rock resistivity.

This model provides an appealing coherent interpretation of the data. In particular, the orders of magnitude of the heat transfer are satisfactory without arbitrary parameters. Therefore, other possible contributions to the thermal budget of the cavity need not be considered at this stage. In particular, natural ventilation (Linden 1999), which plays an important role in underground settings (De Freitas *et al.* 1982; Perrier *et al.* 2002, 2004), is not required here to account for the seasonal evaporation and condensation processes. Natural ventilation is presumably weak in the Aburatsubo vault, but pending experimental assessments it may offer an interesting option for alternative models.

CONCLUSION AND PERSPECTIVES

The analysis of the spatial and temporal temperature variations at the rock–atmosphere interface in the experimental vault at Aburatsubo leads to a qualitative and quantitative physical understanding of the reproducible winter and summer regimes characterizing this site. Thermal signatures support the hypothesis of alternating diffusive and convective water exchange processes. It is important to take into account such processes for the modelling of various parameters recorded in the Aburatsubo observatory such as electrical resistivity, deformation or seismic velocity (Yamamura *et al.* 2003). The origin of the coherent thermal breathing with periods ranging from 1 day to 1 month, in both the winter and summer regimes, remains poorly understood.

Our analysis suggests that the vertical temperature gradient plays an important role in the dynamics of underground cavities. Unfortunately, few high-precision data have been published. Measuring the vertical temperature difference is problematic in general, as high-precision set-ups need to be installed for long periods of time. Punctual measurements usually give erroneous results as the presence of an operator may cause temperature effects larger than the vertical temperature difference, especially near the ceiling, as illustrated in Fig. 8(b). Dedicated and precise experiments should therefore be undertaken in various contexts to measure the vertical temperature gradient.

Water transfer through phase changes has important consequences for the conservation of cave paintings. As an illustration, let us consider a cavity which is located deep enough to be free of seasonal heat flux variations (for example a depth larger than 40 m) and which initially has a negative temperature gradient, with radiative and convective upward thermal transfer of the geothermal heat flow. We can expect an adiabatic temperature gradient in this situation. In such a cavity, water phases do not need to take place, and vertical water flow can be small or even zero. If this cavity now suffers an intrusion due to a human presence, even for a short duration, this causes heating at the ceiling, which can easily reach 0.2 °C, as observed in Aburatsubo, with a recovery time larger than 1 day. If the vertical temperature gradient then becomes positive a downward radiative heat transfer takes place. The only process by which this radiative heat flux can be compensated, to restore the upward geothermal heat flow, is by generating a vertical heat transfer by water exchange. This inversion of the natural temperature gradient hence generates a vertical water flow in the cavity. Furthermore, this positive temperature gradient could be self-stabilizing; the cavity, even if only perturbed for a short amount of time, may not return rapidly to its initial state, and the water flow may continue after the perturbation. As the Aburatsubo data show, not only the ceiling and the floor but also the walls are taking part in the evaporation and condensation process. If the ceiling and walls of the cavity bear precious pre-historic paintings great damage may result, adding to the chemical effect of water and carbon dioxide emitted by the visitors (Sanchez-Moral *et al.* 1999). An underground cavity thus may not be resilient to a transient local heating, even if it is small (100 W) and for a duration of a few hours only. Heating experiments in the underground Vincennes quarry indeed indicate long-term effects and even suggest irreversible temperature changes (Crouzeix *et al.* 2003). Cumulative effects of a similar nature due to visitors have also been reported in painted caves (e.g. Hoyos *et al.* 1997).

Monitoring the atmospheric temperature in a painted cave is largely insufficient for the study of such processes; both the rock temperature and the rock–atmosphere interface must be simultaneously monitored. In the context of painted caves, where it is not permissible to damage the walls by drilling, one could use techniques where the temperature of the interface is sampled by contact only without drilling a hole. Indeed, dedicated experiments performed in a climatic chamber in the context of the preservation of historical monuments have demonstrated that, to a first approximation, the temperature of a rock can be monitored by simple contact, in particular as far as the water flow is concerned (Brüggerhoff *et al.* 2001).

In the context of underground waste repositories, the modification of the water flow pattern by permanent or transient heat sources may result in accelerated degradation processes at ceiling level. If condensation is initiated at the ceiling, in particular, the corrosive properties of pure water may lead to the dissolution of calcite sealing fractures (Morat & Le Mouël 1992; Sanchez-Moral *et al.* 1999). In order to characterize such processes, geochemical methods may be of great help. In general, the underlying dynamics driving the long-term processes in an underground cavity may include important chemical feedback loops, for example through atmospheric CO_2 (Baker & Genty 1998).

Concerning the long-term temperature increase of 0.1 °C observed in Aburatsubo, it is premature to present it as reliable evidence for local or global warming. However, a similar temperature increase has been simultaneously observed at Vincennes (Crouzeix *et al.* 2003). Subsurface monitoring of climate changes certainly appears to be an interesting option.

Beyond geophysical observatories, preservation of painted caves and underground waste storage, underlying physical processes involving compositional buoyancy are important for understanding the dynamics of the atmosphere, the ocean and of the Earth's interior.

ACKNOWLEDGMENTS

The authors thank Y. Ishikawa and M. Serizawa for maintenance of the measurements at the Aburatsubo observatory. This French–Japanese research collaboration was initiated through the bilateral exchange programme between the *Centre National de la Recherche Scientifique* (France) and the *Japan Society for the Promotion of Science* (Japan). Financial support is partly due to the Japanese

Earthquake Prediction Research Programme. This paper is IPGP contribution number 1933.

REFERENCES

Baines, W.D. & Turner, J.S., 1969. Turbulent buoyant convection from a source in a confined region, *J. Fluid Mech.,* **37,** 51–80.

Baker, A. & Genty, D., 1998. Environmental pressures on conserving cave speleothems: effects of changing surface land use and increased cave tourism, *J. Environ. Manage.,* **53,** 165–175.

Birkholzer, J.T. & Tsang, Y.W., 2000. Modeling the thermal-hydrologic processes in a large scale underground heater test in partially saturated fractured tuff, *Water Resources Res.,* **36,** 1431–1447.

Brüggerhoff, S., Wange, G., Morat, P., Le Mouël, J.-L. & Perrier, F., 2001. First results of using combined mass and temperature measurements to study the water flux at the rock-atmosphere interface, *J. Cult. Heritage,* **2,** 117–132.

Crouzeix, C., Le Mouël, J.-L., Perrier, F., Richon, P. & Morat, P., 2003. Long term thermal evolution and effect of low power heating in an underground quarry, *C. R. Geosci.,* **335,** 345–354.

De Freitas, C.R. & Littlejohn, R.N., 1987. Cave climate: assessment of heat and moisture exchange, *J. Climatol.,* **7,** 553–569.

De Freitas, C.R., Littlejohn, R.N., Clarkson, T.S. & Kristament, I. S., 1982. Cave climate: assessment of airflow and ventilation, *J. Climatol.,* **2,** 383–397.

Grossmann, S. & Lohse, D., 2000. Scaling in thermal convection: a unifying theory, *J. Fluid Mech.,* **407,** 27–56.

Grossmann, S. & Lohse, D., 2001. Thermal convection for large Prandtl numbers, *Phys. Rev. Lett.,* **86,** 3316–3319.

Hoyos, M., Soler, V., Cañaveras, J.C., Sanchez-Moral, S., & Sanz-Rubio, E., 1998. Microclimatic characterization of a karstic cave: human impact on microenvironmental parameters of a prehistoric rock art cave (Candamo Cave, northern Spain), *Environ. Geol.,* **33**(4), 231–242.

Linden, P.F., 1999. The fluid mechanics of natural ventilation, *Ann. Rev. Fluid Mech.,* **31,** 201–238.

Morat, P. & Le Mouël, J.-L., 1992. Electrical signals generated by stress variations in porous non saturated rocks, *C. R. Acad. Sci. Paris,* **315,** 955–963.

Morat, P., Le Mouël, J.-L., Poirier, J.-P. & Kossobokov, V., 1999. Heat and water transport by oscillatory convection in an underground cavity, *C. R. Acad. Sci. Paris,* **328,** 1–8.

Musy, A. & Soutter, M., 1991. *Physique du Sol,* Presses Polytechniques et Universitaires Romandes, Lausanne (in French).

Perrier, F., Morat, P. & Le Mouël, J.-L., 2001. Pressure induced temperature variations in an underground quarry, *Earth planet. Sci. Lett.,* **191,** 145–156.

Perrier, F., Morat, P. & Le Mouël, J.-L., 2002. Dynamics of air avalanches in the access pit of an underground quarry, *Phys. Rev. Lett.,* **89,** 134501.

Perrier, F., Richon, P., Crouzeix, C., Morat, P. & Le Mouël, J.-L., 2004. Radon-222 signatures of natural ventilation regimes in an underground quarry, *J. Environ. Radioactiv.,* **71,** 17–32.

Pisarenko, D., Morat, P. & Le Mouël, J.-L., 1996. On a possible mechanism of sandstone alteration: evidence from electric potential measurements, *C. R. Acad. Sci. Paris,* **322,** 17–24.

Sanchez-Moral, S., Soler, V., Cañaveras, J.C., Sanz-Rubio, E., Van Grieken, R. & Gysels, K., 1999. Inorganic deterioration affecting the Altamira Cave, N Spain: quantitative approach to wall-corrosion (solutional etching) processes induced by visitors, *Sci. Total Environ.,* **243/244,** 67–84.

Tsang, Y.W., 2000. A field study for understanding thermally driven coupled processes in partially saturated fractured welded tuff, *Int. J. Rock Mech. Mining Sci.,* **37,** 337–356.

Turcotte, D.L., 1992. *Fractals and Chaos in Geology and Geophysics,* Cambridge University Press, New York.

Utada, H., Yoshino, T., Okubo, T. & Yukutake, T., 1998. Seismic resistivity changes observed at Aburatsubo, Central Japan, revisited, *Tectonophysics,* **299,** 317–331.

Villar, E., Bonet, A., Diaz-Caneja, B., Fernandez, P.L., Gutierrez, I., Quindos, L.S., Solana, J.R. & Soto, J., 1984. Ambient temperature variations in the hall of paintings of Altamira cave due to the presence of visitors, *Cave Sci.,* **11,** 99–104.

Witherspoon, P.A., 2000. The Stripa project, *Int. J. Rock Mech. Mining Sci.,* **37,** 385–396.

Yamamura, K., Sano, O., Utada, H., Takei, Y., Nakao, S. & Fukao, Y., 2003. Long-term observation of in situ seismic velocity and attenuation, *J. geophys. Res.,* **108**(B6), 2317, doi:10.1029/2002JB002005.

Yamazaki, Y., 1975. Precursory and resistivity changes, *Pure appl. Geophys.,* **113,** 219–227.

Yoshino, T., Utada, H. & Yukutake, T., 1998. Variations in earth resistivity at Aburatsubo, Central Japan (1993–1997), *Bull. Earthq. Res. Inst. Univ. Tokyo,* **73,** 1–72.